From Shelfbreak to Shoreline: Coastal Sea Level and Local Ocean Dynamics in the Northwest Atlantic

Carolina M.L. Camargo[1], Christopher G. Piecuch[1], and Britt Raubenheimer[1]

[1]Woods Hole Oceanographic Institution

April 08, 2024

Abstract

Sea-level change threatens the U.S. East Coast. Thus, it is important to understand the underlying causes, including ocean dynamics. Most past studies emphasized links between coastal sea level and local atmospheric variability or large-scale circulation and climate, but possible relationships with local ocean currents over the shelf and slope remain largely unexplored. Here we use 7 years of in-situ velocity and sea-level data to quantify the relationship between northeastern U.S. coastal sea level and variable Shelfbreak Jet transport south of Nantucket Island. At timescales of 1-15 days, southern New England coastal sea level and transport vary in anti-phase, with magnitude-squared coherences of ˜0.5 and admittance amplitudes of ˜0.3 m Sv-1. These results are consistent with a dominant geostrophic balance between along-shelf transport and coastal sea level, corroborating a hypothesis made decades ago that was not tested due to the lack of transport data.

From Shelfbreak to Shoreline: Coastal Sea Level and Local Ocean Dynamics in the Northwest Atlantic

C. M. L. Camargo[1], C. G. Piecuch[1], B. Raubenheimer[2]

[1]Physical Oceanography Department, Woods Hole Oceanographic Institution, Woods Hole, United States
[2]Applied Ocean Physics and Engineering Department, Woods Hole Oceanographic Institution, Woods Hole, United States

Key Points:

- Daily Shelfbreak Jet transports and Southern New England coastal sea levels are anti-correlated during 2014-2022.
- The observed relationship between these two variables is consistent with geostrophic balance.
- For this region, coastal sea levels are more sensitive to local ocean dynamics than to large-scale circulation.

Corresponding author: Carolina Camargo, `carolina.camargo@whoi.edu`

Abstract

Sea-level change threatens the U.S. East Coast. Thus, it is important to understand the underlying causes, including ocean dynamics. Most past studies emphasized links between coastal sea level and local atmospheric variability or large-scale circulation and climate, but possible relationships with local ocean currents over the shelf and slope remain largely unexplored. Here we use 7 years of in-situ velocity and sea-level data to quantify the relationship between northeastern U.S. coastal sea level and variable Shelfbreak Jet transport south of Nantucket Island. At timescales of 1–15 days, southern New England coastal sea level and transport vary in anti-phase, with magnitude-squared coherences of $\sim$0.5 and admittance amplitudes of $\sim$0.3 m Sv^{-1}. These results are consistent with a dominant geostrophic balance between along-shelf transport and coastal sea level, corroborating a hypothesis made decades ago that was not tested due to the lack of transport data.

Plain Language Summary

Sea-level rise is an imminent threat to coastal communities worldwide including the U.S. East Coast. Therefore, it is crucial to understand the processes driving regional sea-level change. While past studies documented how coastal sea level may be influenced by large-scale ocean circulation, less attention has been paid to the role of more local currents over the shelf and slope. Here we explore the relationship between coastal sea level along the northeastern U.S. and the Shelfbreak Jet, a current that flows along the shelfbreak from the Labrador Sea to Cape Hatteras (North Carolina). From 7 years of in-situ data of both current velocities and water levels, we see that as coastal sea level rises Shelfbreak Jet transport increases westward (and vice versa) on timescales of days to weeks. Our results lay the groundwork for understanding relationships between coastal sea level and local ocean dynamics elsewhere.

1 Introduction

Sea-level rise is one of the main threats to coastal communities worldwide. Understanding the causes of past coastal sea-level change is critical for constraining sea-level projections and better preparing for the impacts of climate change. In addition to global-mean sea level, coastal sea-level change is affected by spatially varying processes, such as the gravitational, rotational, and deformational effects of water mass redistribution, the inverted-barometer response to changes in air pressure, and ocean dynamics (Stammer et al., 2013). The link between coastal sea level and particular ocean-circulation features is still, in general, poorly understood.

Coastal sea level along northeastern North America has been the subject of many past papers (e.g., Piecuch, 2020, and references therein). Sea level in this region has been mainly related to aspects of large-scale ocean circulation and climate, including the North Atlantic Oscillation (Andres et al., 2013; Kenigson et al., 2018; McCarthy, Haigh, et al., 2015; Woodworth et al., 2017), El Niño-Southern Oscillation (Park & Dusek, 2013; Hamlington et al., 2015), the Atlantic meridional overturning circulation (AMOC, Goddard et al., 2015; Little et al., 2019; Piecuch et al., 2019; Yin et al., 2009; Yin & Goddard, 2013) and the Gulf Stream (Diabaté et al., 2021; Dong et al., 2019). South of Cape Hatteras, coastal sea-level variations have a strong anti-phase relationship with changes in the Gulf Stream transport, across a range of timescales and periods (Montgomery, 1938; Noble & Gelfenbaum, 1992; Park & Sweet, 2015; Stommel, 1958; Thompson, 1986). North of Cape Hatteras, along the Mid-Atlantic Bight and Gulf of Maine, a link between coastal sea level and large-scale open-ocean circulation is less clear. There, local processes over the shelf and slope may exert a stronger influence on sea level (e.g., Noble & Butman, 1979; Piecuch & Ponte, 2015; Sandstrom, 1980; Thompson, 1986; Woodworth et al., 2014). For instance, coastal sea-level variability along the Mid-Atlantic Bight and Gulf of Maine has been related to local along-shore winds (Andres et al., 2013; Chen et al., 2020; Y. Li et al., 2014; Noble & Butman, 1979; Piecuch et al., 2016), changes in local barometric pressure (Piecuch & Ponte, 2015; Zhu et al., 2023), density anomalies originating in the subpolar gyre and Labrador Sea (Dangendorf et al., 2021; Frederikse et al., 2017; Minobe et al., 2017) and river discharges (Piecuch et al., 2018). Other important drivers of sea-level variability in this region may include remote wind and buoyancy forcing (Wang et al., 2022, 2024). However, even models that incorporate all of these effects are unable to fully account for all of the variability present in sea-level observations (e.g., Wang et al., 2022), suggesting that there remains more for us to learn about the drivers of coastal sea level along northeastern North America. Additionally, there have been few attempts to directly relate northeastern North American coastal sea level and local ocean circulation, mainly due to the lack of available observations.

One of the most notable features in the Northwest Atlantic is the aforementioned Gulf Stream (Figure 1), a strong western boundary current that plays a role in both the AMOC and the wind-driven gyre circulation, carrying warm waters from the Florida Strait along the South Atlantic Bight until Cape Hatteras, North Carolina (Andres, 2021; Heiderich & Todd, 2020; Rossby et al., 2014; Stommel, 1958). At Cape Hatteras, the Gulf Stream detaches from the coast and becomes a meandering free jet, flowing eastward into the open ocean, after which two recirculation cells are formed on either side: an anticyclonic cell south of the Gulf Stream over the Sargasso Sea; and a cyclonic cell north of the Gulf Stream over the Slope Sea (Andres et al., 2013, 2020; Csanady & Hamilton, 1988). The latter gyre includes the Slope Current, a relatively strong feature offshore of the shelf (Flagg et al., 2006). Onshore of the slope current, roughly centered over the continental shelbreak, is the Shelfbreak Jet (SBJ), which represents a boundary between fresher nearshore waters and saltier open-ocean waters, and carries cold waters from the Labrador Sea towards Cape Hatteras following the shelfbreak (Flagg et al., 2006; Forsyth et al., 2020; Fratantoni et al., 2001; Fratantoni & Pickart, 2003, 2007; Linder & Gawarkiewicz, 1998). The shelfbreak region is also subject to Gulf Stream rings (Silver et al., 2021), which sometimes interact with the shallow bathymetry, interrupting the SBJ (Forsyth et al., 2022).

Nearly four decades ago, Thompson (1986) hypothesized that the time-variable depth-dependent dynamics of currents over the shelf and upper slope, such as the SBJ, might substantially influence coastal sea-level variability north of Cape Hatteras. This hypothesis, however, has remained largely unexplored due to the lack of observational data. Here we use unprecedentedly long (7-year) observational records of hourly velocity data from the Ocean Observatory Initiative (OOI) Coastal Pioneer Array, together with data from a dense network of coastal tide gauges, to test the hypothesis that coastal sea level is coupled to circulation over the shelf and slope. Our study focuses on characterizing the relationship between the SBJ and sea level along the northeastern United States, with particular emphasis on Southern New England.

2 Material and Methods

2.1 Data

2.1.1 Coastal sea level

We use data from 31 tide-gauge stations along the northeastern United States provided by the NOAA tides and currents portal (Figure 2a, Table S1). Hourly water level (hereinafter sea level) and barometric pressure are downloaded for each station from 2014 until 2023. We use the pressure data to remove the local inverted barometer contribution from the tide-gauge sea-level measurements (Pugh & Woodworth, 2014). Given the large scales of barometric-pressure variability (Figure S1), for stations with incomplete barometric-pressure records, we filled data gaps with a regional average of contempo-

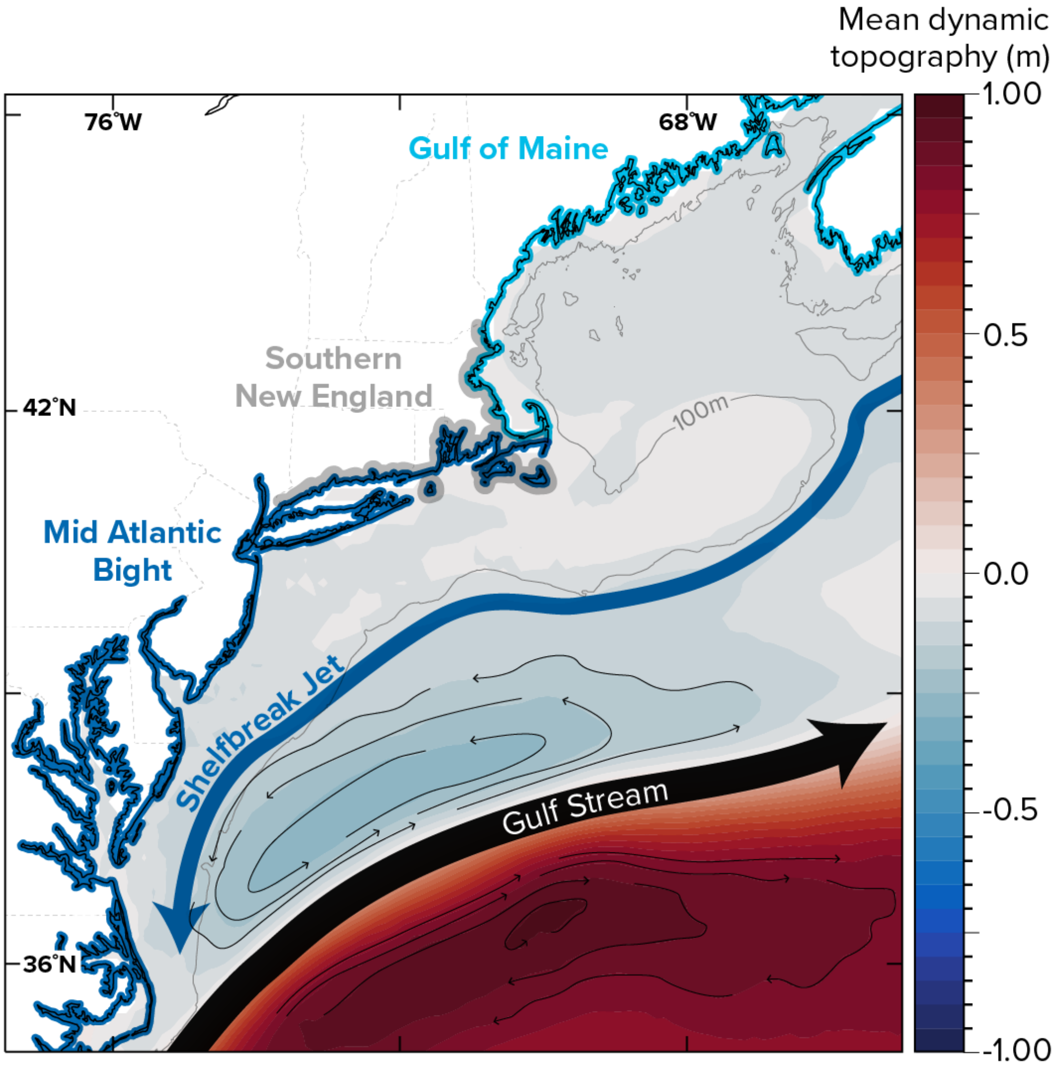

Figure 1. Oceanographic features of the northwestern North Atlantic Ocean. Colors indicate the mean dynamic topography in meters (Jousset, 2023). The mean position of the Gulf Steam and the Shelfbreak Jet are indicated by the black and blue arrows, respectively. The two recirculation cells over the Slope and Sargasso sea are delineated by highs and lows in the mean dynamic topography contour lines. Also indicated in the map is the Gulf of Maine (from Cape Code to Cape Sable Island, Nova Scotia), Mid Atlantic Bight, Southern New England, and the 100-m isobath (light gray line).

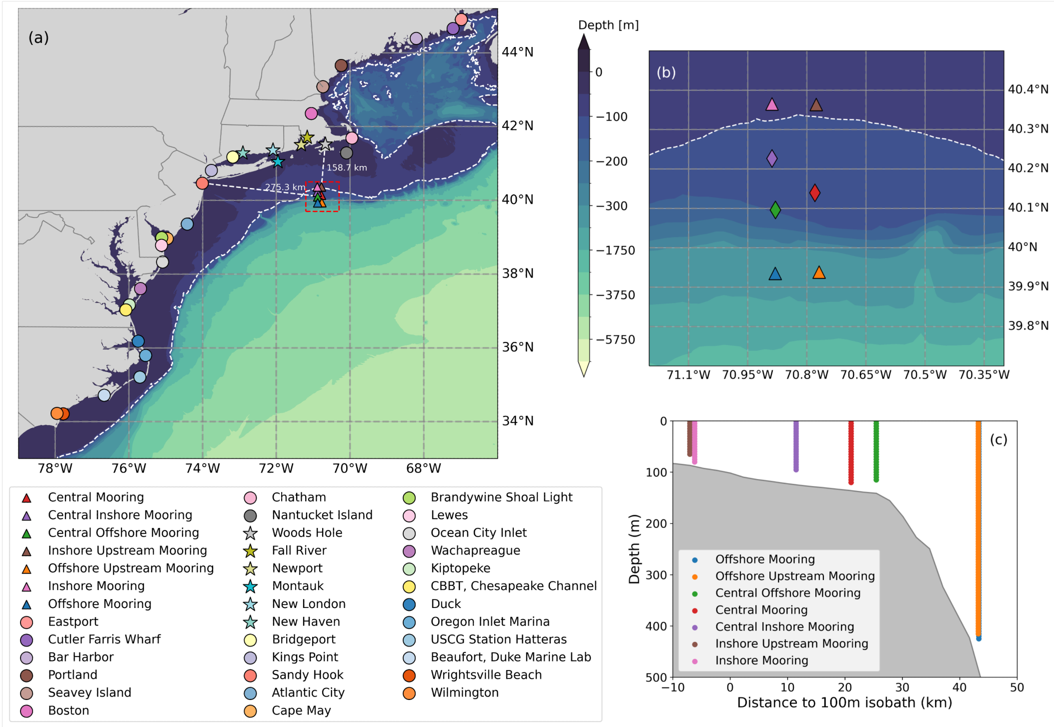

Figure 2. Map of the study area. (a) Regional map showing the locations of tide gauges (filled circles and stars, key at bottom) and of the Pioneer array (filled triangles and diamonds in dashed red box). (b) Zoom-in of the Pioneer array (see red box in a). (c) Depth versus cross-shelf distance of the Pioneer array moorings. Colored contours in (a) and (b) indicate bathymetry (from the General Bathymetric Chart of the Oceans, `https://www.gebco.net/`), and the white dashed line the 100-m isobath. Starred stations in (a) indicate the stations along the Southern New England coast, from which data are averaged in Figures 3 and 5.

raneous barometric-pressure from stations within a 200-km radius. Tides are removed via harmonic analysis (Utide; Codiga, 2011). We use the 68 standard tidal constituents estimated by Utide, except for the solar annual and semiannual astronomical tides, which cannot be distinguished from the mean sea level seasonal cycle driven by wind stress and buoyancy fluxes (e.g., Vinogradov et al., 2008). Other contributions to the sea level signal, such as land motion, mass redistribution and global mean sea-level, are assumed to be negligible on the sub-seasonal timescales examined here.

2.1.2 Shelfbreak Jet velocity and transport

Jet transport is derived using velocity data from the OOI Coastal Pioneer Array (Gawarkiewicz & Plueddemann, 2020). The Array is located at the New England shelfbreak, about 75 nautical miles (∼160 km) south of Martha's Vineyard (Figure 2a), and comprises 7 oceanographic moorings spread from the shelf to offshore of the shelfbreak (Figure 2b,c). The foot of the Shelfbreak Front typically lies between the inshore and central moorings, while the frontal outcrop lies between the central and offshore moorings (Gawarkiewicz & Plueddemann, 2020). Since we want to characterize the SBJ, we use data from the three central moorings, located around the 130-m isobath (127-, 135-, and 147-m water depths) and about 10 to 30 km offshore of the 100-m isobath. Further details can be found in Gawarkiewicz and Plueddemann (2020).

Each mooring has several oceanographic instruments, including a bottom-mounted upward-looking Teledyne RDI Workhorse Acoustic Doppler Current Profiler (ADCP), which measures zonal u (along-shelf, positive east upstream) and meridional v (cross-shelf, positive north onshore) velocities throughout the water column. These are 150-kHz ADCPs, with a burst sampling configuration of 90 pings 2 seconds apart at the top of each hour, that is an hourly sampling frequency of 0.5 Hz and 4-m vertical resolution. Quality controlled data is downloaded from the OOI portal in Earth Coordinates (aligned to geographic north). Although the processed data is provided at 30-minute intervals, we average onto hourly intervals, which is the original temporal resolution, and which is consistent with tide-gauge records. In addition, we grid all ADCP data onto a common vertical axis.

We apply 4 additional criteria to the data. First, we remove instances when less than 80% of the pings within the burst were considered reliable for velocity measurement, considering all 4 beams of the ADCP (Côté et al., 2011). We then remove data from the top 10% of the water column, which is often contaminated by surface reflection, and apply a global range filter, removing any measurements with velocities larger than $\pm$ 2 m s^{-1}. Finally, we remove any time steps with abrupt depth changes, removing erroneous measurements when the ADCP was out of position or inclined.

To reduce the number of gaps in the data and tamp down errors, we compute the regional average of the depth-dependent along-shelf SBJ velocities across the three central moorings. This gives a temporally complete along-shore velocity time series, as a function of depth, from April 2014 until November 2022. Since cross-shore velocity variations are relatively small and along-shore velocities from the individual central moorings are all highly correlated with one another (average Pearson's correlation of 0.8; Figure S2), this averaging process does not introduce appreciable errors. Similarly to the tide gauges, we remove tides via a harmonic analysis (Utide, Codiga (2011)), using the same 66 tidal constituents as before.

Jet transport Q is computed using the depth integral of the zonal velocity u as

$$Q = W \int_{115\text{ m}}^{15\text{ m}} u dz, \tag{1}$$

where W is a jet width scale. We integrate from 15 to 115 m to avoid the surface and bottom layers where there is a lot of missing data. Summing over this depth range returns an integrated velocity that is about 7% smaller than if we included the entire water column. Based on previously reported SBJ transports, we estimate a representative width value of 40 km, which is comparable to previously reported SBJ widths (Table S2; Flagg et al., 2006; Forsyth et al., 2020; Linder & Gawarkiewicz, 1998).

2.2 Spectral analysis

To investigate the relationship between coastal sea level $\eta(t)$ and SBJ transport $Q(t)$, where t is time, we first compute the magnitude-squared coherence $C^2_{Q\eta}(f)$, defined as

$$C^2_{Q\eta}(f) = \frac{|P_{Q\eta}(f)|^2}{P_{\eta\eta} P_{QQ}}, \tag{2}$$

where $P_{\eta Q}(f)$ is the cross-spectral density between $\eta(t)$ and $Q(t)$ at frequency f, and $P_{\eta\eta}(f)$ and $P_{QQ}(f)$ are the respective power spectral densities (Bendat & Piersol, 2010; Quinn & Ponte, 2012; Thomson & Emery, 2014; Vinogradova et al., 2007). The magnitude-squared coherence is the frequency-domain analogue of squared correlation (coefficient of determination) in the time domain. In addition, we compute the admittance (or transfer function), which can be interpreted as a complex-valued regression coefficient computed as a function frequency

$$A_{Q\eta}(f) = \frac{P_{Q\eta}(f)}{P_{QQ}(f)}. \tag{3}$$

Note that, while $C^2_{Q\eta}(f)$ is dimensionless, $A_{Q\eta}(f)$ has dimensions of sea level per transport (m Sv^{-1}). Coherence and admittance are computed with the Scipy package (`https://scipy.org/`). To increase the signal-to-noise ratio for the main timescales of interest (periods between 1 and 15 days), we average over 209 blocks of 360-hour-long segments with a Flattop window and no overlap. Thus, we can resolve periods between 0.08 and 15 days. Note that we tested other analysis choices (e.g., Hann window, 50% overlap), and the results are qualitatively robust (not shown). Confidence level is computed based on Monte Carlo simulation as the 95$^{\mathrm{th}}$ percentile of repeated coherence analyses made on 1000 pairs of random white-noise samples. This gives virtually the same value as textbook estimates based on effective degrees of freedom (0.014, Thomson & Emery, 2014).

To explore the dependence of the coherence and admittance on time interval, we perform wavelet transforms, which can be used to compute both wavelet (magnitude-squared) coherence (Grinsted et al., 2004)

$$WTC_{Q\eta} = \frac{|W_n^{Q\eta}(s)|^2}{W_n^{\eta}(s)W_n^{Q}(s)}, \tag{4}$$

and admittance (Audet, 2011)

$$WTA_{Q\eta} = \frac{W_n^{Q\eta}(s)}{W_n^{Q}(s)}. \tag{5}$$

Here $W_n^x(s)$ is the continuous wavelet transform of a single time series x, $W_n^{xy}(s)$ is the cross-wavelet transform between two time series x and y, n is dimensionless time, and (s) is the scale stretching time (Grinsted et al., 2004). The wavelet coherence and admittance can be thought of as localized frequency-domain analogues of squared correlation and regression coefficient, respectively (Grinsted et al., 2004; Stark et al., 2003). We use Grinsted et al. (2004)'s wavelet package, with a Morlet Wavelet and smoothing of 1/12 scales per octave. Significance levels are based on repeated Monte Carlo simulations with 1000 randomly generated time series.

3 Results

Daily sea level averaged along the Southern New England coast and SBJ transport are anti-correlated over the 7-year study period (Figure 3a). Considering all timescales in the data, we compute a Pearson correlation of −0.54, and a regression coefficient of −0.17 m Sv^{-1} between the two records. Given the westward sense of SBJ flows, this indicates that sea level tends to rise by 17 cm for a 1 Sv increase in SBJ transport, and vice versa for a sea-level fall and SBJ-transport decrease. The relationship between coastal sea level and SBJ transport is more clearly visualized in Figure 3b, which presents a zoom-in on a shorter period. Note that the summers of 2014 and 2015 are exceptions to the rule, when sea level and SBJ transport are uncorrelated, and some prominent transport fluctuations are not mirrored in sea level (Figure S3). While both time series vary over a range of timescales, both show a clear seasonality, particularly in terms of a seasonal oscillation in the magnitudes of daily-to-weekly variability, with stronger variability over the winter months. In fact, high-frequency variability explains a substantial portion of the total data variance. For example, 66% and 43% of the daily sea-level and transport variance, respectively, is explained by variability at periods between 1 and 15 days (Figure 3e,f). Indeed, isolating the 1–15-day band, we obtain stronger correlation (0.61) and regression (-0.27 m Sv^{-1}) coefficients between sea level and SBJ transport (Figure 3e). Therefore, we pay particular, but not exclusive, attention to high frequencies in what follows.

Magnitude squared-coherence and admittance between SBJ transport and Southern New England coastal sea level vary substantially with frequency (Figure 3c). Coherence hovers around zero for timescales shorter than the inertial period (∼19 hours), but values become larger at lower frequencies, for example, increasing from 0.25 at 1-day period to 0.45 at 15-day period. Coherence peaks at 0.53 at 36-hour period, with corresponding admittance magnitude of 0.29 m Sv^{-1}. Note that while the coherence is almost always statistically significant (95% confidence level is 0.014), only higher coherence levels should be interpreted as physically significant. For example, a coherence of 0.3 means that for a certain frequency, one variable can explain 30% of the variance in the other variable at that frequency. For periods between 2 and 4 days, the coherence decreases to 0.36, while the admittance shows a small increase reaching 0.32. For periods longer than 4 days, coherence reaches a plateau around 0.45, while the admittance decreases to 0.25. The admittance phase reveals that both variables are anti-phased, with a phase of 180 degrees for periods larger than 1 day (Figure 3d). These admittance and coherence values are roughly consistent with the signs and magnitudes of the correlation and regression coefficients given earlier. The anti-phase relationship between sea level and SBJ transport at periods longer than $\sim$1 day is consistent with a general expectation for a dominant geostrophic balance at timescales longer than inertial.

Coherence and admittance between SBJ transport and individual tide-gauge records along the northeastern United States show a clear frequency-dependent spatial structure (Figure 4). Peak coherence occurs first and with stronger magnitude at the stations closer to the Array, along the Southern New England coast. Further from it, smaller peaks appear towards lower frequencies. At periods from 1 to 2 days, the stations from Woods Hole to Kings Point show higher coherence, with admittances varying from 0.22 to 0.39 m Sv^{-1}. However, geographic distance alone does not entirely explain the observed patterns, since the Nantucket Island and Chatham stations, which are also relatively close to Pioneer, show lower coherence for this period, indicating that other processes around Nantucket are important for determining sea-level variations in these locations on these timescales.

For periods between 2 to 4 days, the area of higher coherence (> 0.3) extends downstream to Delaware Bay (Lewes). This is the range of periods with the strongest admittance values, varying from 0.24 to 0.41 m Sv^{-1}. The 2–4-day period is comparable to the time it would take a signal to propagate from the Pioneer Array to Delaware Bay at a nominal Kelvin wave speed of 2–3 m s^{-1} (Hughes et al., 2019). For periods from 4 to 15 days, higher coherence extends even further afield, reaching from the Gulf of Maine (Cutler Farris Wharf) down to North Carolina (Duck). We see no physically significant coherence at any frequency downstream of Cape Hatteras (note that our analysis does not include stations farther south than North Carolina). This suggests that the SBJ dynamics influence on sea level simply do not extend farther south or that other factors are more important to sea-level variability in that region (e.g., coastal geometry, proximity of the Gulf Stream to shore).

Wavelet coherence between Southern New England coastal sea level and SBJ transport is generally intermittent and in anti-phase (Figure 5). That is, for some frequency bands, sea level and SBJ transport are significantly coherent during some time intervals but not others. These complex, granular patterns are smoothed out in the block-averaged picture painted by the earlier coherence analysis (Figure 3). We see a strong seasonal modulation of higher-frequency (1–46 day) coherence, which is weak and mostly insignificant in the summer (June to August) and stronger and largely significant in winter (November to February). However, the admittance at 20–40-day periods is lower than at 1–15-day period, suggesting that sea level is less sensitive to SBJ transports at these longer periods. This is consistent with our earlier finding that correlation and regression coefficients between sea level and SBJ transport are higher when we bandpass the data to isolate variability at 1–15-day periods. Times when sea level and SBJ transport are coherent at periods between 10 to 30 days might also be connected to intrusion of warm core rings onto the shelf, which have an average advective time scale of about 30 days, and are known to disrupt the SBJ (Forsyth et al., 2022). Another noticeable feature is the strong coherence in 2018 at 40–180-day period with duration of almost a full year.

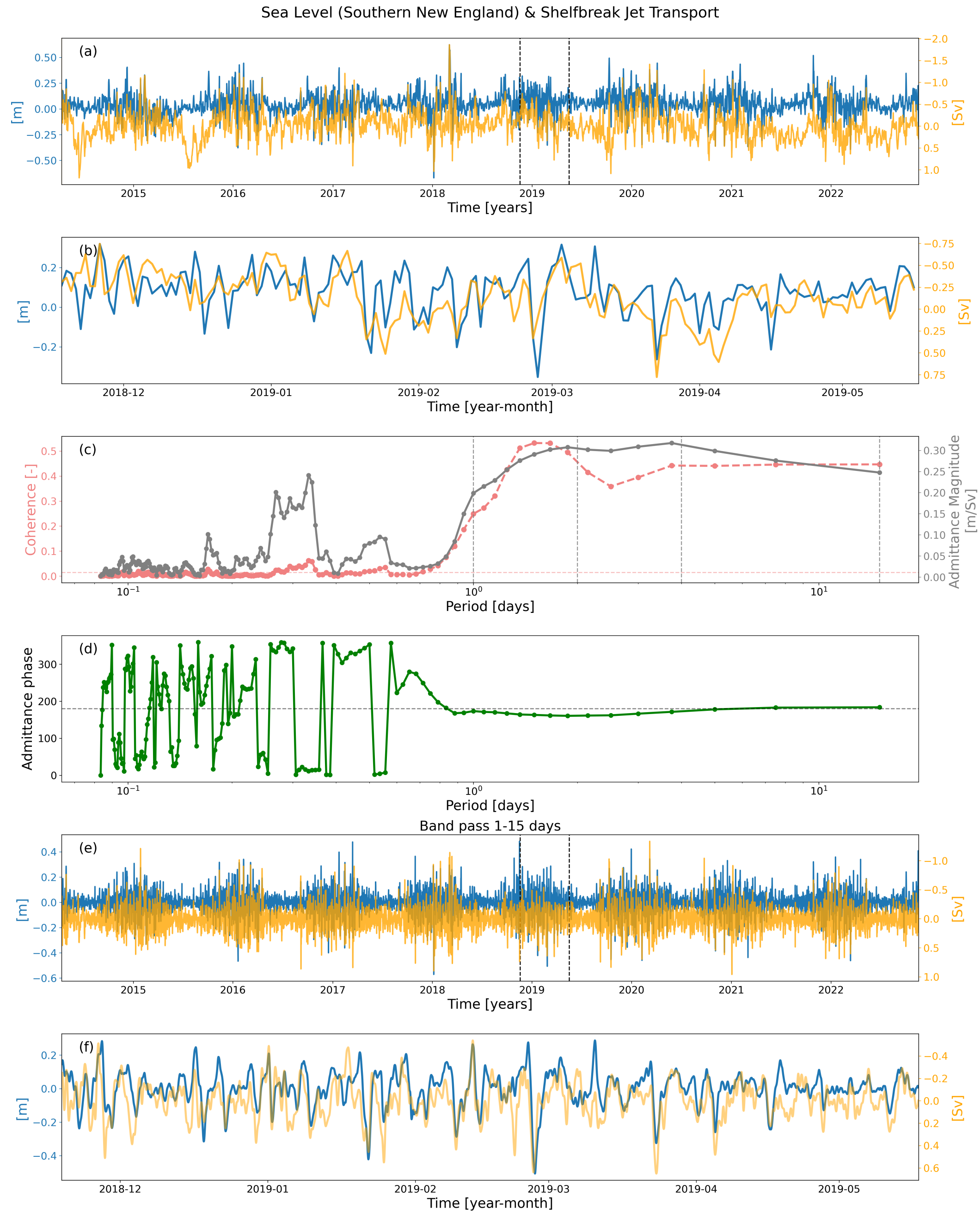

Figure 3. Time series of daily sea level along the Southern coast of New England (blue line, left axis, meters), and of Shelfbreak Jet (SBJ) transport (orange line, right axis, Sv) for the entire record (a) and for 180 days (b) during the period between the vertical dotted lines in (a). (c) Coherence (pink, left axis) and admittance magnitude (gray, right axis, in m Sv^{-1}) between sea level and SBJ transport time series versus period. Horizontal dashed line indicates the 95% confidence level, and vertical lines indicate, from left to right, 1-, 2-, 4-, and 15-day periods. (d) Admittance phase (degrees) versus period. Hourly time series band-passed over 1–15 days for the entire record (e) and for the 180 days (f) delineated by the vertical dotted lines in (e). The right vertical axis in (a), (b), (f), and (e), regarding SBJ time series, is inverted, emphasizing that a negative SBJ anomaly is related to a positive sea-level anomaly.

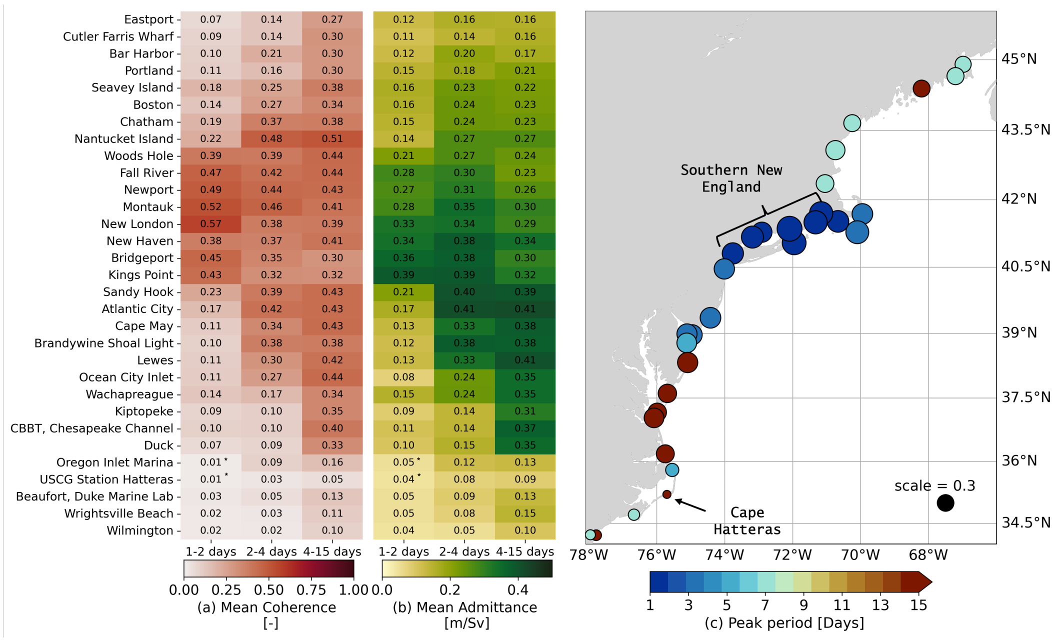

Figure 4. Mean magnitude-squared coherence (a, left) and admittance amplitude (b, middle) between Shelfbreak Jet transport and sea level at tide gauges ranging from Eastport, Maine (top row) down to Wrightville Beach, North Carolina (last row), averaged between 1 to 2 days (left column), 2 to 4 days (middle column) and 4 to 15 days (right columns), with the tide gauges ordered following the coastline from North to South. Asterisk indicates statistically insignificant values. Regional map (c, right) indicating the period (color) and magnitude (size) of maximum coherence. Key locations used for interpretation are indicated in the map.

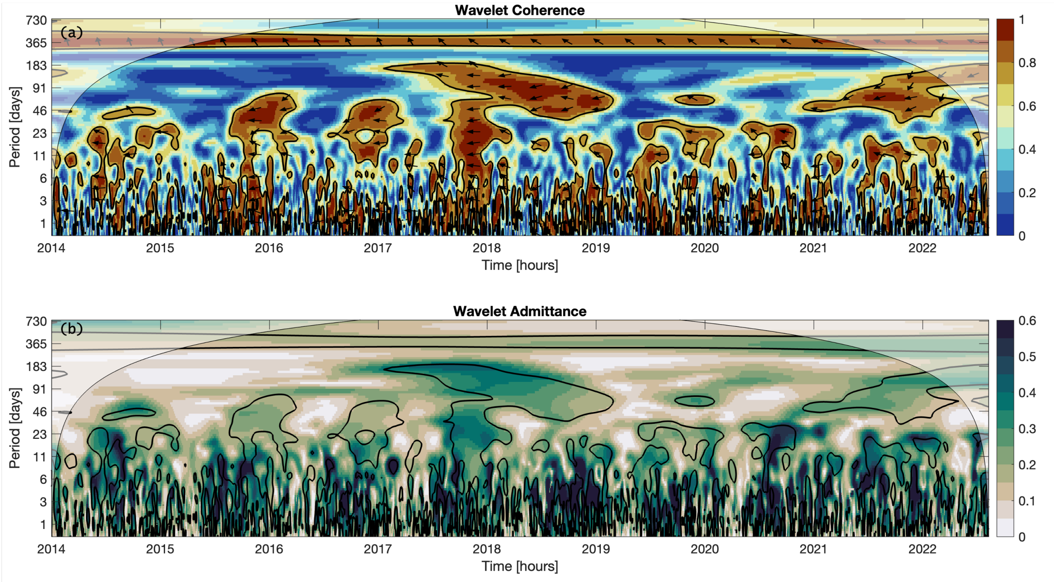

Figure 5. Wavelet coherence (a, top) and admittance (b, bottom) between sea level and Shelfbreak Jet transport. Vertical axis is the period in days, and admittance in m Sv^{-1}. Black contour lines indicate significant area at 95% confidence. Black arrows show the wavelet phase, with right and left arrows indicating in-phase and anti-phase, respectively, and up and down arrows indicating quadrature.

Finally, there is significant coherence during all time intervals at the annual period, but admittance amplitudes are low and the phase indicates more of a quadrature relationship, which is inconsistent with a dominant geostrophic balance.

4 Discussion

In this work we characterized the relationship between coastal sea level along the Northwest Atlantic and the SBJ transport based on observations. We found that coastal sea level along Southern New England is significantly coherent with SBJ transport at 1–15-day periods, with coherence between the signals extending farther along the coast for the longer periods. This unique analysis of multi-year records of local circulation and coastal sea level allowed us to corroborate a hypothesis made decades ago that had never been tested. Our findings provide valuable insight and complement past studies by shedding light on processes contributing to sea-level changes that were previously overlooked, serving as a reference point for understanding similar phenomena in different regions.

Our results are roughly consistent with expectations from ocean dynamics. Bingham and Hughes (2009) made a thermal-wind argument that the sensitivity of coastal sea level to alongshore upper-ocean transport is $-2f/gH$, where f is the Coriolis parameter, g is gravity, and H is the thickness of the upper ocean layer. Using $H = 80$ m based on the mean grounding position of the SBJ, we obtain a sensitivity of -0.25 m Sv^{-1}, which roughly agrees in sign and order of magnitude with our results (Figure 3). Note that this crude estimate ignores important details of bathymetric variation. In contrast, the sensitivity of coastal sea level to a variation in AMOC transport is approximately -0.02 m Sv^{-1} (Little et al., 2019, and references therein), an order of magnitude smaller than with the SBJ. That is, Southern New England sea level is more sensitive to variations in SBJ transport than to equal transport variations in the AMOC. However, SBJ transport fluctuations are about an order of magnitude or so smaller than AMOC transport variations (Forsyth et al., 2020; McCarthy, Smeed, et al., 2015). Thus, the respective dynamics of the SBJ and AMOC may have comparable influences on coastal sea level.

Geostrophic balance is a diagnostic relationship, not a statement of cause and effect. Thus, our results do not suggest that transport changes drive sea-level changes (or vice versa), but rather suggest that common drivers induce variations in both SBJ and coastal sea level. For example, local wind forcing might explain the tandem fluctuations of sea level and the jet transport, as discussed in previous studies (e.g., Noble & Butman, 1979; Noble & Gelfenbaum, 1992; Sandstrom, 1980). The observed covariance between SBJ transport and coastal sea level may also be tied to instabilities of the shelf-break front or the Gulf Stream. For example, the average instability (meandering) time scale of the SBJ ranges from about 4 to 15 days (Fratantoni & Pickart, 2003; Garvine et al., 1988; Gawarkiewicz, 1991; Gawarkiewicz et al., 2004; Lozier et al., 2002). Thus, the high coherence on the 1–15-day band could be linked to the meandering time scale of the SBJ. Likewise, influences of Gulf-Stream rings and instabilities interacting with the bathymetry of the continental margin may also be relevant (e.g., Cherian & Brink, 2016, 2018). Furthermore, the spatial pattern of significant coherence might be related to the coastline geometry, or to the influence of winds in the region, which strengthen the SBJ between Nantucket and Long Island Sound (Lobert et al., 2023). For example, south of the Hudson Canyon (New Jersey), the dominant wind direction changes, which could explain why coherence between 1–2 days is lower in this region. Future studies should interrogate the forcing and dynamics mediating the relationship between the SBJ and sea level, which is important to understand to what extent coarse-resolution climate models, that do not resolve the SBJ, accurately simulate coastal sea level.

We demonstrated that SBJ transport and sea level are coherent across a range of timescales. This implies that changes in one variable are partly informative of changes in the other. Since only short records of SBJ transport exist, one might use the longer tide-gauge time series, which are available for some locations going back more than a century, to reconstruct some aspects of past SBJ variability. While the amount of variability we can reconstruct may be limited, future studies could also incorporate other variables relevant to the SBJ, such as temperature and salinity. Such an effort may, if successful, be informative for determining whether contemporary coastal ocean changes are anomalous in a wider historical context (e.g., Piecuch, 2020, and references therein).

Our results also have implications for coastal flooding studies. The frequency of high-tide flooding is rapidly increasing along the U.S. coasts (Moftakhari et al., 2015), making it important that we understand all the factors that contribute to such events. Customarily, the different components affecting coastal water levels are identified largely through harmonic analysis and filtering techniques, which enables the effects of mean sea-level changes to be distinguished from astronomical tides and storm surges (e.g., Sun et al., 2023; S. Li et al., 2022). Here, however, we illustrated that SBJ-related variability is relevant at timescales of 1 to 15 days, which roughly coincides with the storm surge frequency band. Thus, it is important to determine to what extent SBJ dynamics are interwoven with more familiar storm-surge processes related to winds, waves, and pressure, and to what extent SBJ processes play a role in high-tide flooding.

In addition to SBJ transport, sea level may also be sensitive to other aspects of SBJ variability, such as meandering, broadening or narrowing of the jet and cross-shore movement (Wise et al., 2018). However, the fixed position of the moorings does not allow an exploration of all these variables. Future studies using higher spatial resolution datasets, such as ocean models and satellite products, could investigate how coastal sea level responds to variations in jet position and width. More generally, our study demonstrates the value of sustained, continuous coastal ocean observing of the shelf and slope for understanding the dynamics of coastal sea-level variability.

Open Research Section

Tide gauge data is available at https://tidesandcurrents.noaa.gov/stations.html?type=Water+Levels (last accessed March/2024), and specific tide gauges names in Table S1. Pioneer Array data at the OOI Portal (https://ooinet.oceanobservatories.org/, last accessed March/2024). Specific links to central moorings ADCPs are: https://ooinet.oceanobservatories.org/data_access/?search=CP02PMCI-RII01-02-ADCPTG010 (Central Inshore Profiler Mooring); https://ooinet.oceanobservatories.org/data_access/?search=CP02PMCO-RII01-02-ADCPTG010 (Central Offshore Profiler Mooring); https://ooinet.oceanobservatories.org/data_access/?search=CP01CNSM-MFD35-01-ADCPTF000 (Central Surface Mooring). The quality controlled Shelfbreak Jet transport time series is available at https://doi.org/10.5281/zenodo.10814048 (Camargo, 2024).

Acknowledgments

C.M.L.C. was supported by funds from the Francis E. Fowler IV Center for Ocean and Climate at Woods Hole Oceanographic Institution. C.G.P. was supported by the NASA Sea Level Change Team (grant 80NSSC20K1241), Ocean Surface Topography Science Team (Jet Propulsion Laboratory Subcontract 1670515), and the National Science Foundation (award OCE-2123692). B.R. was supported by the National Science Foundation (award OCE-1848650). Figure 1 was produced by Natalie Renier (WHOI Creative Studio). This material is based upon work supported by the Ocean Observatories Initiative (OOI), a major facility fully funded by the National Science Foundation under Cooperative Agreement No. 1743430, and the Woods Hole Oceanographic Institution OOI Program Office.

References

Andres, M. (2021, September). Spatial and Temporal Variability of the Gulf Stream Near Cape Hatteras. *Journal of Geophysical Research: Oceans*, *126*(9), e2021JC017579. doi: 10.1029/2021JC017579

Andres, M., Donohue, K. A., & Toole, J. M. (2020, February). The Gulf Stream's path and time-averaged velocity structure and transport at 68.5°W and 70.3°W. *Deep Sea Research Part I: Oceanographic Research Papers*, *156*, 103179. doi: 10.1016/j.dsr.2019.103179

Andres, M., Gawarkiewicz, G. G., & Toole, J. M. (2013, November). Interannual sea level variability in the western North Atlantic: Regional forcing and remote response. *Geophysical Research Letters*, *40*(22), 5915–5919. doi: 10.1002/2013GL058013

Audet, P. (2011, January). Directional wavelet analysis on the sphere: Application to gravity and topography of the terrestrial planets. *Journal of Geophysical Research*, *116*(E1), E01003. doi: 10.1029/2010JE003710

Bendat, J. S., & Piersol, A. G. (2010). *Random Data: Analysis and Measurement Procedures* (1st ed.). Wiley. doi: 10.1002/9781118032428

Bingham, R. J., & Hughes, C. W. (2009, January). Signature of the Atlantic meridional overturning circulation in sea level along the east coast of North America. *Geophysical Research Letters*, *36*(2), 2008GL036215. doi: 10.1029/2008GL036215

Camargo, C. M. L. (2024, March). *Shelfbreak jet transport from OOI pioneer.* Zenodo. doi: 10.5281/zenodo.10814048

Chen, N., Han, G., & Yan, X.-H. (2020). Similarity and Difference in Interannual Sea Level Variations Between the Mid-Atlantic Bight and the Nova Scotia Coast. *Journal of Geophysical Research: Oceans*, *125*(5), e2019JC015919. doi: 10.1029/2019JC015919

Cherian, D. A., & Brink, K. H. (2016, December). Offshore Transport of Shelf Water by Deep-Ocean Eddies. *Journal of Physical Oceanography*, *46*(12), 3599–3621. doi: 10.1175/JPO-D-16-0085.1

Cherian, D. A., & Brink, K. H. (2018, May). Shelf Flows Forced by Deep-Ocean Anticyclonic Eddies at the Shelf Break. *Journal of Physical Oceanography*, *48*(5), 1117–1138. doi: 10.1175/JPO-D-17-0237.1

Codiga, D. L. (2011). *Unified Tidal Analysis and Prediction Using the UTide Matlab Functions* (Tech. Rep. No. GSO Technical Report 2011-01). Narragansett, RI.: Graduate School of Oceanography, University of Rhode Island.

Côté, J. M., Hotchkiss, F. S., Martini, M., & Denham, C. R. (2011). *Acoustic Doppler Current Profiler (ADCP) Data Processing System Manual* (Tech. Rep. Nos. 00–458). Reston, Virginia: U.S. Geological Survey.

Csanady, G., & Hamilton, P. (1988, May). Circulation of slopewater. *Continental Shelf Research*, *8*(5-7), 565–624. doi: 10.1016/0278-4343(88)90068-4

Dangendorf, S., Frederikse, T., Chafik, L., Klinck, J. M., Ezer, T., & Hamlington, B. D. (2021, June). Data-driven reconstruction reveals large-scale ocean circulation control on coastal sea level. *Nature Climate Change*, *11*(6), 514–520. doi: 10.1038/s41558-021-01046-1

Diabaté, S. T., Swingedouw, D., Hirschi, J. J.-M., Duchez, A., Leadbitter, P. J., Haigh, I. D., & McCarthy, G. D. (2021, April). Western boundary circulation and coastal sea-level variability in northern hemisphere oceans. *Ocean Science*, *17*, 1449–1417. doi: 10.5194/os-17-1449-2021

Dong, S., Baringer, M. O., & Goni, G. J. (2019, April). Slow Down of the Gulf Stream during 1993–2016. *Scientific Reports*, *9*(1), 6672. doi: 10.1038/s41598-019-42820-8

Flagg, C. N., Dunn, M., Wang, D.-P., Rossby, H. T., & Benway, R. L. (2006, June). A study of the currents of the outer shelf and upper slope from a decade of shipboard ADCP observations in the Middle Atlantic Bight.

Journal of Geophysical Research: Oceans, *111*(C6), 2005JC003116. doi: 10.1029/2005JC003116

Forsyth, J., Andres, M., & Gawarkiewicz, G. (2020, September). Shelfbreak Jet Structure and Variability off New Jersey Using Ship of Opportunity Data From the *CMV* Oleander. *Journal of Geophysical Research: Oceans*, *125*(9), e2020JC016455. doi: 10.1029/2020JC016455

Forsyth, J., Gawarkiewicz, G., & Andres, M. (2022, March). The Impact of Warm Core Rings on Middle Atlantic Bight Shelf Temperature and Shelf Break Velocity. *Journal of Geophysical Research: Oceans*, *127*(3), e2021JC017759. doi: 10.1029/2021JC017759

Fratantoni, P. S., & Pickart, R. S. (2003, May). Variability of the shelf break jet in the Middle Atlantic Bight: Internally or externally forced? *Journal of Geophysical Research: Oceans*, *108*(C5), 2002JC001326. doi: 10.1029/2002JC001326

Fratantoni, P. S., & Pickart, R. S. (2007, October). The Western North Atlantic Shelfbreak Current System in Summer. *Journal of Physical Oceanography*, *37*(10), 2509–2533. doi: 10.1175/JPO3123.1

Fratantoni, P. S., Pickart, R. S., Torres, D. J., & Scotti, A. (2001, August). Mean Structure and Dynamics of the Shelfbreak Jet in the Middle Atlantic Bight during Fall and Winter*. *Journal of Physical Oceanography*, *31*(8), 2135–2156. doi: 10.1175/1520-0485(2001)031⟨2135:MSADOT⟩2.0.CO;2

Frederikse, T., Simon, K., Katsman, C. A., & Riva, R. (2017, July). The sea-level budget along the N orthwest A tlantic coast: GIA , mass changes, and large-scale ocean dynamics. *Journal of Geophysical Research: Oceans*, *122*(7), 5486–5501. doi: 10.1002/2017JC012699

Garvine, R. W., Wong, K.-C., Gawarkiewicz, G. G., McCarthy, R. K., Houghton, R. W., & Aikman, F. (1988, December). The morphology of shelfbreak eddies. *Journal of Geophysical Research: Oceans*, *93*(C12), 15593–15607. doi: 10.1029/JC093iC12p15593

Gawarkiewicz, G. (1991, April). Linear Stability Models of Shelfbreak Fronts. *Journal of Physical Oceanography*, *21*.

Gawarkiewicz, G., Brink, K. H., Bahr, F., Beardsley, R. C., Caruso, M., Lynch, J. F., & Chiu, C.-S. (2004, March). A large-amplitude meander of the shelfbreak front during summer south of New England: Observations from the Shelfbreak PRIMER experiment. *Journal of Geophysical Research: Oceans*, *109*(C3), 2002JC001468. doi: 10.1029/2002JC001468

Gawarkiewicz, G., & Plueddemann, A. J. (2020, January). Scientific rationale and conceptual design of a process-oriented shelfbreak observatory: The OOI Pioneer Array. *Journal of Operational Oceanography*, *13*(1), 19–36. doi: 10.1080/1755876X.2019.1679609

Goddard, P. B., Yin, J., Griffies, S. M., & Zhang, S. (2015, February). An extreme event of sea-level rise along the Northeast coast of North America in 2009–2010. *Nature Communications*, *6*(1), 6346. doi: 10.1038/ncomms7346

Grinsted, A., Moore, J. C., & Jevrejeva, S. (2004, November). Application of the cross wavelet transform and wavelet coherence to geophysical time series. *Nonlinear Processes in Geophysics*, *11*(5/6), 561–566. doi: 10.5194/npg-11-561-2004

Hamlington, B. D., Leben, R. R., Kim, K.-Y., Nerem, R. S., Atkinson, L. P., & Thompson, P. R. (2015). The effect of the El Niño-Southern Oscillation on U.S. regional and coastal sea level. *Journal of Geophysical Research: Oceans*, *120*(6), 3970–3986. doi: 10.1002/2014JC010602

Heiderich, J., & Todd, R. E. (2020, August). Along-Stream Evolution of Gulf Stream Volume Transport. *Journal of Physical Oceanography*, *50*(8), 2251–2270. doi: 10.1175/JPO-D-19-0303.1

Hughes, C. W., Fukumori, I., Griffies, S. M., Huthnance, J. M., Minobe, S., Spence, P., ... Wise, A. (2019, November). Sea Level and the Role of Coastal Trapped Waves in Mediating the Influence of the Open Ocean on the Coast. *Surveys in Geophysics*, *40*(6), 1467–1492. doi: 10.1007/s10712-019-09535-x

Jousset, S. (2023). *Mean Dynamic Topography MDT CNES_CLS 2022.* CNES. doi: 10.24400/527896/A01-2023.003

Kenigson, J. S., Han, W., Rajagopalan, B., Yanto, & Jasinski, M. (2018, July). Decadal Shift of NAO-Linked Interannual Sea Level Variability along the U.S. Northeast Coast. *Journal of Climate*, *31*(13), 4981–4989. doi: 10.1175/JCLI-D-17-0403.1

Li, S., Wahl, T., Barroso, A., Coats, S., Dangendorf, S., Piecuch, C., ... Liu, L. (2022). Contributions of Different Sea-Level Processes to High-Tide Flooding Along the U.S. Coastline. *Journal of Geophysical Research: Oceans*, *127*(7), e2021JC018276. doi: 10.1029/2021JC018276

Li, Y., Ji, R., Fratantoni, P. S., Chen, C., Hare, J. A., Davis, C. S., & Beardsley, R. C. (2014). Wind-induced interannual variability of sea level slope, along-shelf flow, and surface salinity on the Northwest Atlantic shelf. *Journal of Geophysical Research: Oceans*, *119*(4), 2462–2479. doi: 10.1002/2013JC009385

Linder, C. A., & Gawarkiewicz, G. (1998, August). A climatology of the shelfbreak front in the Middle Atlantic Bight. *Journal of Geophysical Research: Oceans*, *103*(C9), 18405–18423. doi: 10.1029/98JC01438

Little, C. M., Hu, A., Hughes, C. W., McCarthy, G. D., Piecuch, C. G., Ponte, R. M., & Thomas, M. D. (2019, September). The Relationship Between U.S. East Coast Sea Level and the Atlantic Meridional Overturning Circulation: A Review. *Journal of Geophysical Research: Oceans*, *124*(9), 6435–6458. doi: 10.1029/2019JC015152

Lobert, L., Gawarkiewicz, G., & Plueddemann, A. (2023, July). Categorization of High-Wind Events and Their Contribution to the Seasonal Breakdown of Stratification on the Southern New England Shelf. *Journal of Geophysical Research: Oceans*, *128*(7), e2022JC019625. doi: 10.1029/2022JC019625

Lozier, M. S., Reed, M. S. C., & Gawarkiewicz, G. G. (2002, March). Instability of a Shelfbreak Front. *Journal of Physical Oceanography*, *32*(3), 924–944. doi: 10.1175/1520-0485(2002)032⟨0924:IOASF⟩2.0.CO;2

McCarthy, G. D., Haigh, I. D., Hirschi, J. J.-M., Grist, J. P., & Smeed, D. A. (2015, May). Ocean impact on decadal Atlantic climate variability revealed by sea-level observations. *Nature*, *521*(7553), 508–510. doi: 10.1038/nature14491

McCarthy, G. D., Smeed, D. A., Johns, W. E., Frajka-Williams, E., Moat, B. I., Rayner, D., ... Bryden, H. L. (2015, January). Measuring the Atlantic Meridional Overturning Circulation at 26°N. *Progress in Oceanography*, *130*, 91–111. doi: 10.1016/j.pocean.2014.10.006

Minobe, S., Terada, M., Qiu, B., & Schneider, N. (2017, May). Western Boundary Sea Level: A Theory, Rule of Thumb, and Application to Climate Models. *Journal of Physical Oceanography*, *47*(5), 957–977. doi: 10.1175/JPO-D-16-0144.1

Moftakhari, H. R., AghaKouchak, A., Sanders, B. F., Feldman, D. L., Sweet, W., Matthew, R. A., & Luke, A. (2015). Increased nuisance flooding along the coasts of the United States due to sea level rise: Past and future. *Geophysical Research Letters*, *42*(22), 9846–9852. doi: 10.1002/2015GL066072

Montgomery, R. (1938, January). Fluctuations in monthly sea level on eastern U.S. coast as related to dynamics of western North Atlantic Ocean. *Journal of Marine Research*, *1*(2).

Noble, M. A., & Butman, B. (1979). Low-frequency wind-induced sea level oscillations along the east coast of North America. *Journal of Geophysical Research: Oceans*, *84*(C6), 3227–3236. doi: 10.1029/JC084iC06p03227

Noble, M. A., & Gelfenbaum, G. R. (1992). Seasonal fluctuations in sea level on the South Carolina shelf and their relationship to the Gulf Stream. *Journal of*

Geophysical Research: Oceans, *97*(C6), 9521–9529. doi: 10.1029/92JC00811
Park, J., & Dusek, G. (2013, June). ENSO components of the Atlantic multidecadal oscillation and their relation to North Atlantic interannual coastal sea level anomalies. *Ocean Science*, *9*(3), 535–543. doi: 10.5194/os-9-535-2013
Park, J., & Sweet, W. (2015, July). Accelerated sea level rise and Florida Current transport. *Ocean Science*, *11*(4), 607–615. doi: 10.5194/os-11-607-2015
Piecuch, C. G. (2020). Drivers of US East Coast sea-level variability from years to decades in a changing ocean— What do we know and what do we need to know? *US Clivar Variations*, *18*(3).
Piecuch, C. G., Bittermann, K., Kemp, A. C., Ponte, R. M., Little, C. M., Engelhart, S. E., & Lentz, S. J. (2018, July). River-discharge effects on United States Atlantic and Gulf coast sea-level changes. *Proceedings of the National Academy of Sciences*, *115*(30), 7729–7734. doi: 10.1073/pnas.1805428115
Piecuch, C. G., Dangendorf, S., Gawarkiewicz, G. G., Little, C. M., Ponte, R. M., & Yang, J. (2019, May). How is New England Coastal Sea Level Related to the Atlantic Meridional Overturning Circulation at 26° N? *Geophysical Research Letters*, *46*(10), 5351–5360. doi: 10.1029/2019GL083073
Piecuch, C. G., Dangendorf, S., Ponte, R. M., & Marcos, M. (2016, July). Annual Sea Level Changes on the North American Northeast Coast: Influence of Local Winds and Barotropic Motions. *Journal of Climate*, *29*(13), 4801–4816. doi: 10.1175/JCLI-D-16-0048.1
Piecuch, C. G., & Ponte, R. M. (2015, July). Inverted barometer contributions to recent sea level changes along the northeast coast of North America. *Geophysical Research Letters*, *42*(14), 5918–5925. doi: 10.1002/2015GL064580
Pugh, D., & Woodworth, P. (2014). *Sea-Level Science: Understanding Tides, Surges, Tsunamis and Mean Sea-Level Changes.* Cambridge: Cambridge University Press. doi: 10.1017/CBO9781139235778
Quinn, K. J., & Ponte, R. M. (2012, April). High frequency barotropic ocean variability observed by GRACE and satellite altimetry. *Geophysical Research Letters*, *39*(7), 2012GL051301. doi: 10.1029/2012GL051301
Rossby, T., Flagg, C. N., Donohue, K., Sanchez-Franks, A., & Lillibridge, J. (2014, January). On the long-term stability of Gulf Stream transport based on 20 years of direct measurements. *Geophysical Research Letters*, *41*(1), 114–120. doi: 10.1002/2013GL058636
Sandstrom, H. (1980, January). On the wind-induced sea level changes on the Scotian shelf. *Journal of Geophysical Research: Oceans*, *85*(C1), 461–468. doi: 10.1029/JC085iC01p00461
Silver, A., Gangopadhyay, A., Gawarkiewicz, G., Silva, E. N. S., & Clark, J. (2021, January). Interannual and seasonal asymmetries in Gulf Stream Ring Formations from 1980 to 2019. *Scientific Reports*, *11*(1), 2207. doi: 10.1038/s41598-021-81827-y
Stammer, D., Cazenave, A., Ponte, R. M., & Tamisiea, M. E. (2013, January). Causes for Contemporary Regional Sea Level Changes. *Annual Review of Marine Science*, *5*(1), 21–46. doi: 10.1146/annurev-marine-121211-172406
Stark, C. P., Stewart, J., & Ebinger, C. J. (2003, December). Wavelet transform mapping of effective elastic thickness and plate loading: Validation using synthetic data and application to the study of southern African tectonics. *Journal of Geophysical Research: Solid Earth*, *108*(B12), 2001JB000609. doi: 10.1029/2001JB000609
Stommel, H. (1958). *The Gulf Stream: A Physical and Dynamical Description.* Berkeley, Los Angeles and London: University of California Press and Cambridge University Press.
Sun, Q., Dangendorf, S., Wahl, T., & Thompson, P. R. (2023, December). Causes of accelerated High-Tide Flooding in the U.S. since 1950. *npj Climate and Atmospheric Science*, *6*(1), 210. doi: 10.1038/s41612-023-00538-5

Thompson, K. R. (1986, October). North Atlantic sea-level and circulation. *Geophysical Journal International*, *87*(1), 15–32. doi: 10.1111/j.1365-246X.1986.tb04543.x

Thomson, R. E., & Emery, W. J. (2014). Data Analysis Methods in Physical Oceanography. In *Data Analysis Methods in Physical Oceanography* (Third ed., p. iii). Elsevier. doi: 10.1016/B978-0-12-387782-6.01001-2

Vinogradov, S. V., Ponte, R. M., Heimbach, P., & Wunsch, C. (2008). The mean seasonal cycle in sea level estimated from a data-constrained general circulation model. *Journal of Geophysical Research: Oceans*, *113*(C3). doi: 10.1029/2007JC004496

Vinogradova, N. T., Ponte, R. M., & Stammer, D. (2007, February). Relation between sea level and bottom pressure and the vertical dependence of oceanic variability. *Geophysical Research Letters*, *34*(3), 2006GL028588. doi: 10.1029/2006GL028588

Wang, O., Lee, T., Frederikse, T., Ponte, R. M., Fenty, I., Fukumori, I., & Hamlington, B. D. (2024, January). What Forcing Mechanisms Affect the Interannual Sea Level Co-Variability Between the Northeast and Southeast Coasts of the United States? *Journal of Geophysical Research: Oceans*, *129*(1), e2023JC019873. doi: 10.1029/2023JC019873

Wang, O., Lee, T., Piecuch, C. G., Fukumori, I., Fenty, I., Frederikse, T., … Zhang, H. (2022, June). Local and Remote Forcing of Interannual Sea-Level Variability at Nantucket Island. *Journal of Geophysical Research: Oceans*, *127*(6), e2021JC018275. doi: 10.1029/2021JC018275

Wise, A., Hughes, C. W., & Polton, J. A. (2018, December). Bathymetric Influence on the Coastal Sea Level Response to Ocean Gyres at Western Boundaries. *Journal of Physical Oceanography*, *48*(12), 2949–2964. doi: 10.1175/JPO-D-18-0007.1

Woodworth, P. L., Maqueda, M. A. M., Roussenov, V. M., Williams, R. G., & Hughes, C. W. (2014, December). Mean sea-level variability along the northeast A merican A tlantic coast and the roles of the wind and the overturning circulation. *Journal of Geophysical Research: Oceans*, *119*(12), 8916–8935. doi: 10.1002/2014JC010520

Woodworth, P. L., Morales Maqueda, M. A., Gehrels, W. R., Roussenov, V. M., Williams, R. G., & Hughes, C. W. (2017, October). Variations in the difference between mean sea level measured either side of Cape Hatteras and their relation to the North Atlantic Oscillation. *Climate Dynamics*, *49*(7-8), 2451–2469. doi: 10.1007/s00382-016-3464-1

Yin, J., & Goddard, P. B. (2013). Oceanic control of sea level rise patterns along the East Coast of the United States. *Geophysical Research Letters*, *40*(20), 5514–5520. doi: 10.1002/2013GL057992

Yin, J., Schlesinger, M. E., & Stouffer, R. J. (2009, April). Model projections of rapid sea-level rise on the northeast coast of the United States. *Nature Geoscience*, *2*(4), 262–266. doi: 10.1038/ngeo462

Zhu, Y., Han, W., & Alexander, M. A. (2023). Nonstationary Roles of Regional Forcings in Driving Low-Frequency Sea Level Variability Along the U.S. East Coast Since the 1950s. *Geophysical Research Letters*, *50*(15), e2023GL104191. doi: 10.1029/2023GL104191

Supporting Information for "From Shelfbreak to Shoreline: Coastal Sea Level and Local Ocean Dynamics in the Northwest Atlantic"

C. M. L. Camargo[1], C. G. Piecuch[1], B. Raubenheimer[2]

[1]Physical Oceanography Department, Woods Hole Oceanographic Institution, Woods Hole, United States

[1]Applied Ocean Physics and Engineering Department, Woods Hole Oceanographic Institution, Woods Hole, United States

Contents of this file

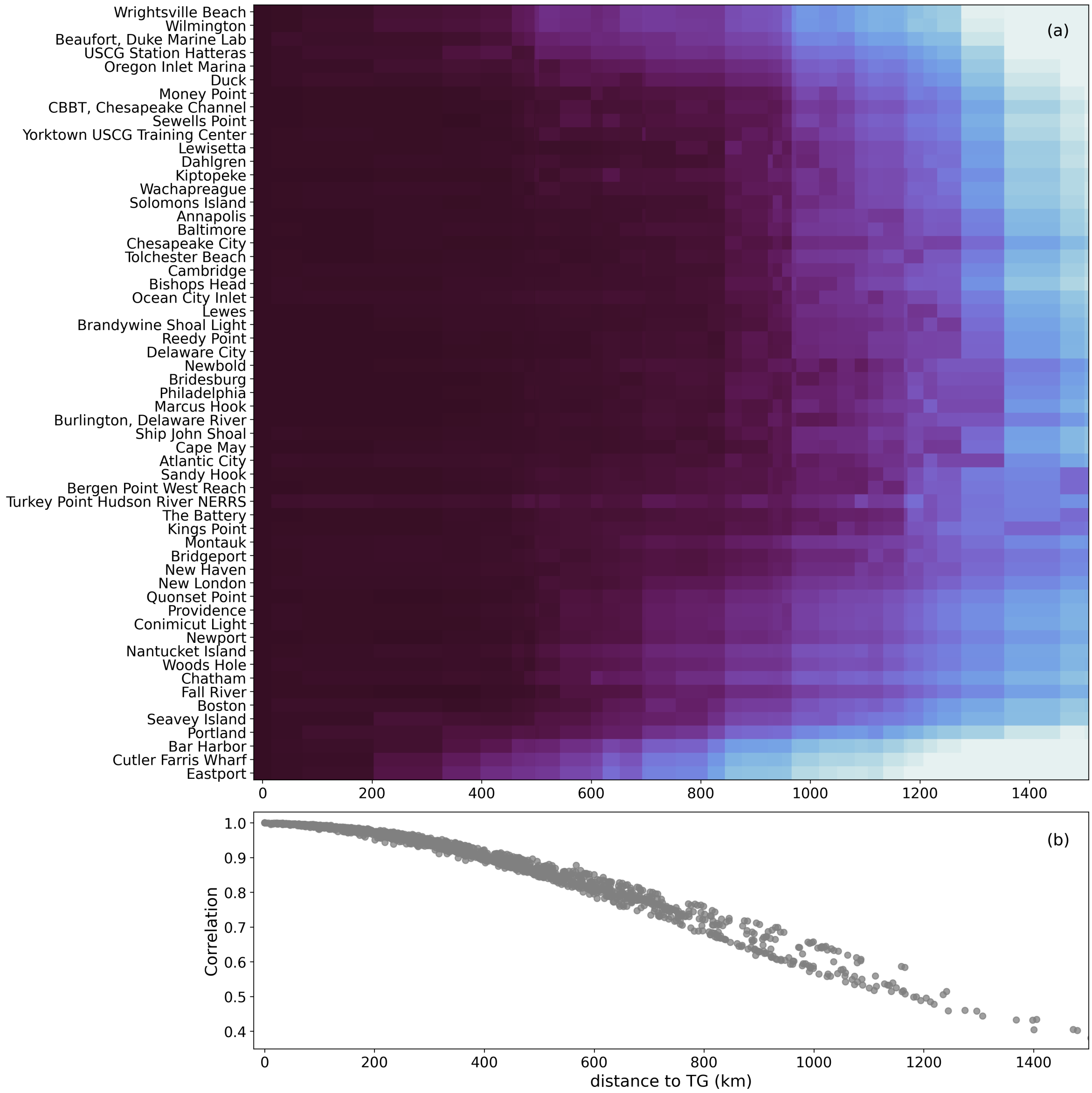

Figure S1. Pair-wise correlation between the atmospheric pressure at each tide gauge station. (a) Heat map and (b) scatter plot of the correlations versus distance between the tide gauges. Both plots highlight the spatial fingerprint of the atmospheric pressure: stations within 200km of one another have similar variability with the correlation falling below 0.5 for distances greater than about 800 km.

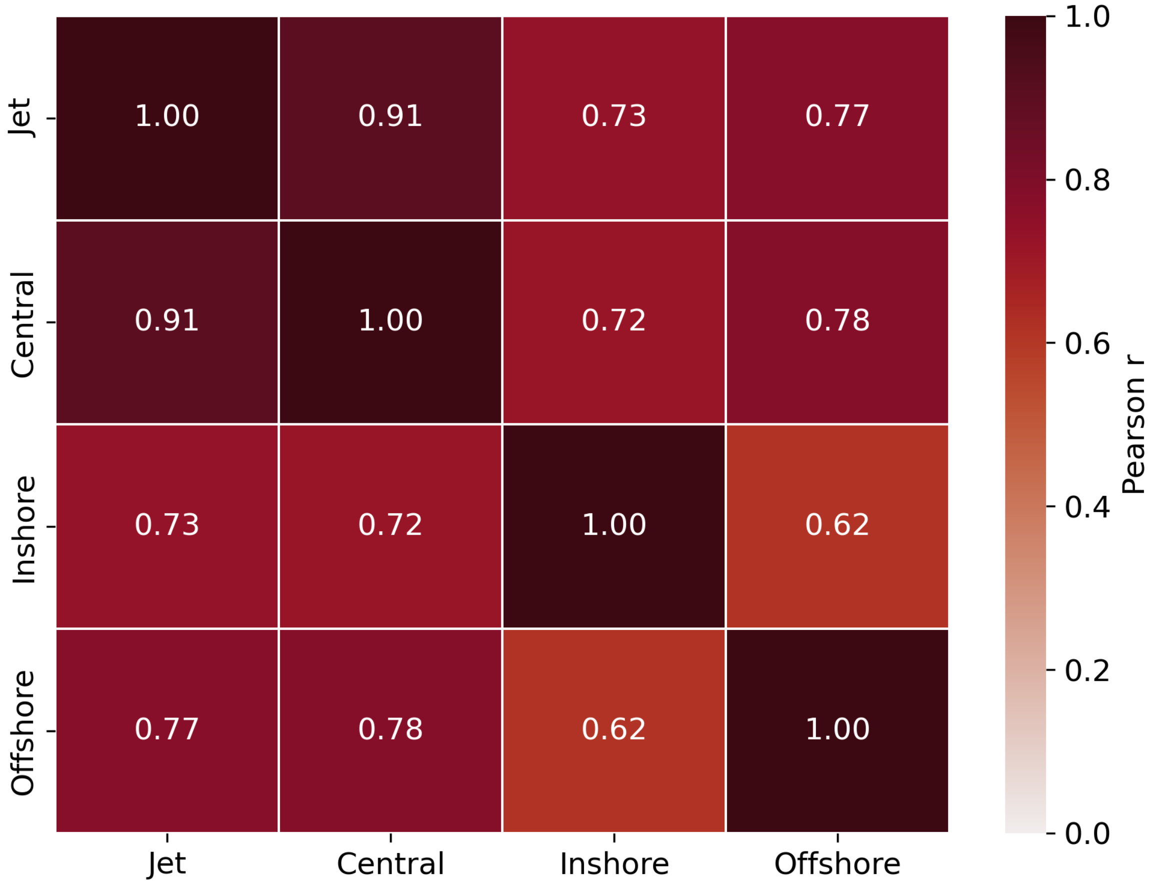

Figure S2. Heat map of the correlation between the regional composite of the jet and the three central moorings of the Pioneer Array. The highest correlation of the jet average is with the central mooring. The central mooring also has high correlation with both the inshore and the offshore moorings. The lowest correlation is between the inshore and offshore moorings, which are 14.3km apart (0.62).

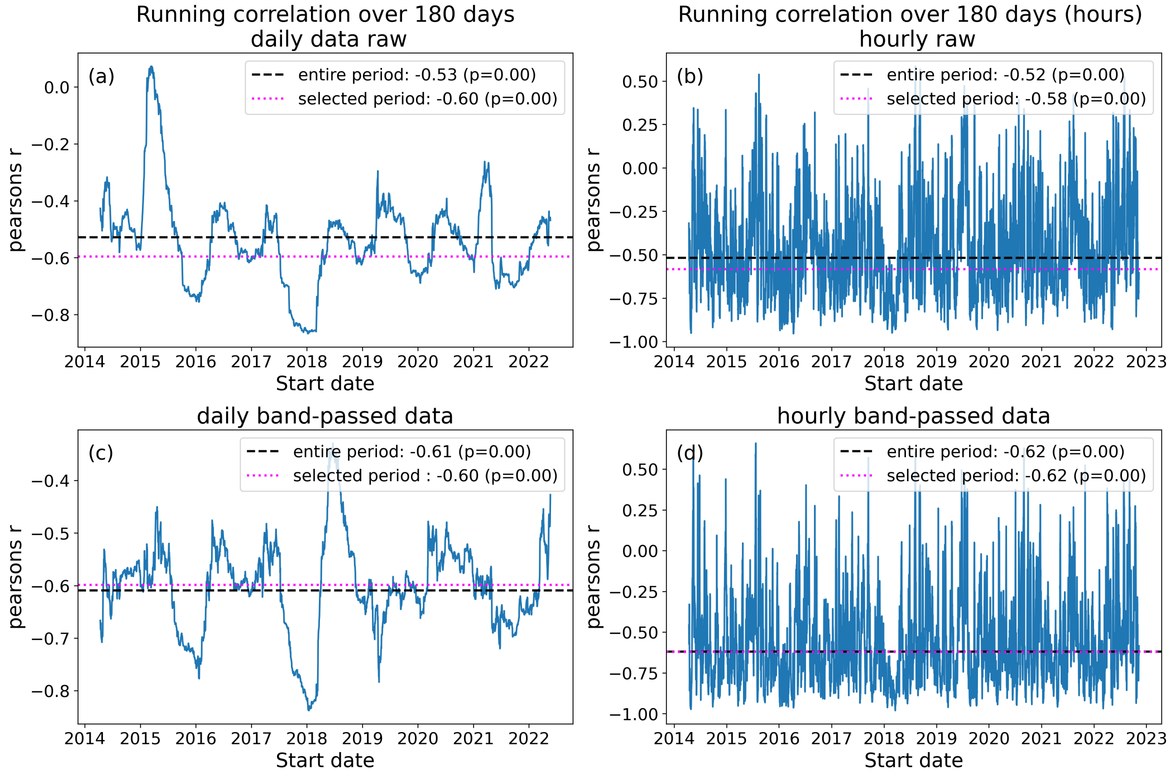

Figure S3. 6-months running correlation between the coastal sea level along Southern New England and the Shelfbreak Jet transport, for daily raw data (a), hourly raw data (b), daily 1–15-day band-passed data (c) and hourly 1–15-day band-passed data (d). Black dashed line indicates the correlation for the entire time series, and pink dotted line the correlation for the selected period shown in Figure 3b,f.

Table S1. Metadata table of tide gauge stations used in this work. Completeness level refers to gaps in the sea-level height data between April 2014 to November 2022. Note that a larger gap will influence the degrees of freedom of the spectral analysis and its significance level. For example, the coherence of a complete time series has a 95% confidence level of 0.014, while Seavey Island has a confidence level of 0.05, using blocks of 360 segments for averaging.

Station	Latitude [°]	Longitude [°]	Completeness [%]
Eastport	44.90	-66.98	100.0
Cutler Farris Wharf	44.66	-67.20	100.0
Bar Harbor	44.39	-68.20	99.0
Portland	43.66	-70.24	100.0
Seavey Island	43.08	-70.74	28.0
Boston	42.35	-71.05	100.0
Chatham	41.69	-69.95	82.0
Nantucket Island	41.29	-70.10	100.0
Woods Hole	41.52	-70.67	100.0
Fall River	41.70	-71.16	100.0
Newport	41.50	-71.33	100.0
Montauk	41.05	-71.96	98.0
New London	41.36	-72.09	99.0
New Haven	41.28	-72.91	100.0
Bridgeport	41.18	-73.18	99.0
Kings Point	40.81	-73.76	100.0
Sandy Hook	40.47	-74.01	100.0
Atlantic City	39.36	-74.42	100.0
Cape May	38.97	-74.96	100.0
Brandywine Shoal Light	38.99	-75.11	81.0
Lewes	38.78	-75.12	100.0
Ocean City Inlet	38.33	-75.09	100.0
Wachapreague	37.61	-75.69	100.0
Kiptopeke	37.17	-75.99	100.0
CBBT, Chesapeake Channel	37.03	-76.08	65.0
Duck	36.18	-75.75	100.0
Oregon Inlet Marina	35.80	-75.55	99.0
USCG Station Hatteras	35.21	-75.70	99.0
Beaufort, Duke Marine Lab	34.72	-76.67	100.0
Wrightsville Beach	34.21	-77.79	97.0
Wilmington	34.23	-77.95	100.0

Table S2. Previously reported values of SBJ transport (Q) used to obtain the width scaling factor (W'). The width scale of 40km used here is the average of all W', obtained by diving transport Q by the mean depth-integrated velocity of our jet velocities (6.8 $m^2.s^{-1}$). Note that most of the studies focused on the jet farther south than our study region, offshore of New Jersey. Forsyth et al. (2020) provides measurements in both Eulerian and Stream coordinates, indicated by superscript ^{e} and ^{s}. For comparison, we also have the reported widths of each study (W), defined by Forsyth et al. (2020) and Flagg et al. (2006) as the e-folding width of the jet, and as the contour of half of the maximum surface velocity by (Linder & Gawarkiewicz, 1998).

Reference	Year	Location	Q (Sv)	W' (km)	W (km)
Linder and Gawarkiewicz (1998)	1900-1990	Nantucket Shoals	0.24	35.2	21
Linder and Gawarkiewicz (1998)	1900-1990	New Jersey	0.16	23.5	19
Forsyth et al. (2020)^e	1994-2018	New Jersey	$0.21 \pm .02$	30.8	50
Forsyth et al. (2020)^s	1994-2018	New Jersey	$0.37 \pm .04$	54.3	40
Flagg et al. (2006)	1994-2002	New Jersey	0.4	58.7	30

References

Flagg, C. N., Dunn, M., Wang, D.-P., Rossby, H. T., & Benway, R. L. (2006, June). A study of the currents of the outer shelf and upper slope from a decade of shipboard ADCP observations in the Middle Atlantic Bight. *Journal of Geophysical Research: Oceans*, *111*(C6), 2005JC003116. doi: 10.1029/2005JC003116

Forsyth, J., Andres, M., & Gawarkiewicz, G. (2020, September). Shelfbreak Jet Structure and Variability off New Jersey Using Ship of Opportunity Data From the *CMV* Oleander. *Journal of Geophysical Research: Oceans*, *125*(9), e2020JC016455. doi: 10.1029/2020JC016455

Linder, C. A., & Gawarkiewicz, G. (1998, August). A climatology of the shelfbreak front in the Middle Atlantic Bight. *Journal of Geophysical Research: Oceans*, *103*(C9), 18405–18423. doi: 10.1029/98JC01438